ELSEVIER

Journal of Nuclear Materials 274 (1999) 320–328

journal of nuclear materials

www.elsevier.nl/locate/jnucmat

Deposition of lithium on a plasma edge probe in TFTR. Behavior of lithium-painted walls interacting with edge plasmas [1]

Y. Hirooka [a,*], K. Ashida [b], H. Kugel [c], D. Walsh [d], W. Wampler [d], M. Bell [c], R. Conn [a], M. Hara [b], S. Luckhardt [a], M. Matsuyama [b], D. Mansfield [c], D. Mueller [c], C. Skinner [c], T. Walters [c], K. Watanabe [b]

[a] *University of California, San Diego, 9500 Gilman Dr., La Jolla, CA 92093-0417, USA*
[b] *Toyama University, Gofuku 3190, Toyama 930, Japan*
[c] *Princeton University, P.O. Box 451, Princeton, NJ 08543, USA*
[d] *Sandia National Laboratories, Albuquerque, NM 87185-5800, USA*

Received 18 May 1998; accepted 28 January 1999

Abstract

Recent observations have indicated that lithium pellet injection wall conditioning plays an important role in achieving the enhanced supershot regime in TFTR (the tokamak test fusion reactor). However, little is understood about the behavior of lithium-coated limiter walls, interacting with edge plasmas. In the final campaign of TFTR, a cylindrical carbon fiber composite probe was inserted into the boundary plasma region and exposed to ohmically heated deuterium discharges with lithium pellet injection. The ion-drift side probe surface exhibits a sign of codeposition of lithium, carbon, oxygen, and deuterium, whereas the electron side essentially indicates high-temperature erosion. It is found that lithium is incorporated in these codeposits in the form of oxide at the concentration of a few percent. In the electron side, lithium has been found to penetrate deeply into the probe material, presumably via rapid diffusion through interplane spaces in the graphite crystalline. Though it is not conclusive, materials mixing in the carbon and lithium system appears to be a key process to successful lithium wall conditioning.

1. Introduction

It is widely recognized that wall conditioning is essential in achieving high-performance plasma confinement in a magnetic fusion device. To review recent achievements in fusion research, one cannot ignore the role wall conditioning has played. These include the supershot mode in TFTR by helium discharge conditioning [1], the VH-mode in DIII-D by the combination of boronization and helium conditioning [2], and most recently the enhanced-supershot mode in pre-boronized TFTR by lithium pellet injection [3]. Among all the wall conditioning techniques applied in TFTR, lithium conditioning is the only one with which the energy confinement time has significantly been increased [4].

To interpret briefly these wall conditioning effects, helium discharge conditioning depletes the plasma-interactive walls of previously implanted fuel particles, which then results in reduced edge recycling in the following shots. Boronized walls have been found to capture large amount of fuel particles as well as impurities [5]. It immediately follows from these arguments that the combination of boronization and helium conditioning can provide further improvement. However, the effect of lithium pellet injection has not yet been well interpreted to date.

* Corresponding author. Present address: National Institute for Fusion Science, 322-6 Oroshi-cho, Toki, Japan. Tel.: +81-572 58 2256; fax: +81-572 58 2628; e-mail: hirooka@nifs.ac.jp

[1] This paper was presented at the 13th International Conference on Plasma Surface Interactions in Controlled Fusion Devices, San Diego, CA, 18–22 May 1998.

0022-3115/99/$ – see front matter
PII: S0022-3115(99)00053-7

The effect of lithium pellet injection on the plasma performance in TFTR was first accidentally discovered in 1990 [3]. Since then much has been demonstrated about beneficial effects of lithium-coated first walls in TFTR [4]. In contrast, lithium injection has only brought modest improvement to other confinement devices, including DIII-D [6], JIPP-IIU [7], TdeV [8] and ALCATOR C-Mod [9]. First-order explanation is that all these devices run divertor discharges, meaning that by nature the effect of first walls is minimal, no matter how they are conditioned. Nevertheless, the question remains open as to how lithium-coated walls interact with edge plasmas.

In the meantime, plasma-facing materials mixing came up as a new issue in the fusion community with the advent of the ITER divertor cassette design in which beryllium, carbon and tungsten are employed for in-vessel components, positioned closely one another. However, this is not a specific issue of ITER. To the contrary, one finds a variety of materials mixing opportunities in other fusion devices as well, either in operation or under design. From this materials mixing point of view, TFTR provides a rather interesting opportunity, mixing of lithium with deuterium, tritium, and carbon from the underlying graphite tiles, together with other impurities such as oxygen.

In this work, a deposition probe positioned in the boundary region of TFTR has been exposed to fiducial deuterium–deuterium (D–D) discharges with lithium pellet injection in January 1997. Extensive materials analysis has been done on this probe, using a variety of materials analysis techniques, to find out about spatial distributions and chemical states of mixed materials of lithium, tritium, deuterium, lithium, oxygen, carbon and other impurities. This paper is intended to report the essence of these materials analysis data and to discuss possible mechanisms, affecting the plasma interaction behavior with the lithium-coated first walls in TFTR. Comprehensive data sets obtained from these individual analysis techniques will be published separately [10,11].

2. Experimental

The deposition probe used in this work is a machined piece of a CFC (carbon fiber composite) material from FMI (Fiber Materials Inc.), in the form of cylinder with the length of 9.1 cm and the diameter of 5.6 cm. This CFC material has a four-directionally woven fiber structure and the impurity contents are listed in Table 1. On 31 January 1997 in the final campaign of TFTR, 6 OH (ohmically heated) discharge cleaning shots were done with helium. The probe was then inserted into the boundary region through the Bay-D port located at $R = 2.624$ m and exposed to OH D–D discharges with lithium pellet injection.

In these three D–D shots, the discharge parameters are: plasma heating power of 1 MW; plasma current of 1.6 mA; edge safety factor of about 4; major radius of 2.6 m and minor radius of 0.95 m. The deposition probe is thus positioned 2.4 cm off the poloidal center of the plasma. As to the vertical position, in the minor radius direction, the probe top surface was set at about 2 cm off the last closed flux surface. The flat-top duration was about 3 s during which lithium pellets were injected individually with some intervals in-between. The number of injected pellets are 2, 4 and 4, respectively, for these discharges. The pellet is in the form of cylinder with the diameter of about 2 mm and the length of about 2 mm, containing 3 mg of lithium (i.e., 3×10^{20} Li-atoms). Following these successful D–D discharges, the last one was disrupted right after the first pellet was injected. However, the disruption effect on the probe experiment is expected to be minimal because statistically in TFTR,

Table 1
Impurity contents in the C–C composite used for the probe

Impurity element	Contents (ppm)		
	FMI TFTR-probe	ToyoTanso	
		IG-43	IG-430U
B	17	3	0.1
Na	<10	<0.5	<0.002
Al	5–24	14	<0.001
Si	<50	2	<0.1
K	<50	2	<0.03
Ca	<10	6	<0.01
Ti	1.7	33	<0.001
V	10.9	40	<0.001
Cr	0.3	<0.3	<0.004
Fe	10	26	<0.02
Ni	<0.5	4	<0.001

Note: (1) IG-43 is a general purpose graphite and IG-430U is an ultra-high purity graphite for special purposes, used in JT-60U and LHD; (2) No significant difference as to other impurity elements.

the stored energy release is directed towards the bumper limiter. The total number of injected pellets was 11, meaning 3.3×10^{21} Li-atoms, which provides an average lithium coverage of 1 monolayer/cm^2 over the TFTR internal surface area. It is important to mention here that the injected lithium was enriched with Li-6 to 95.6% in this campaign to avoid resonance absorption of the RF heating power.

After it was extracted from the TFTR system, the probe was immediately subjected to smear tests for tritium monitoring to ensure the safety. The probe was then transported in an argon-purged container to Sandia National Labs. and NRA (nuclear reaction analysis) was performed on 14 March 1997, using the X-IBA (external ion beam analysis) facility. For this analysis it is not necessary to section the probe, so that the elemental mapping of lithium and deuterium was performed over the entire surface. The nuclear reactions used in this analysis are: ^{7}Li(p, α)α and ^{3}He(d, p)α, the former of which means that the analysis was performed on the diluted lithium isotope.

The probe was then sent overseas to Toyama University Hydrogen Isotope Research Centre where tritium-compatible XPS (X-ray induced photoelectron spectroscopy) and SIMS (secondary ion mass spectrometry) are available. On 2 July 1997, the probe was cut into small specimens for a series of XPS-SIMS measurements. After this the probe was transported back to the UCSD-Fusion Laboratory and surface morphology analysis with SEM (scanning electron microscopy) was conducted on 4 December 1997. Due to the limited machine time on these material analysis facilities, as will be seen in the following sections, effort was concentrated on the comparison in surface characteristics between the ion drift side vs. electron drift side of the plasma-front surface of the probe.

3. Results and discussion

3.1. Evaluation of edge plasma conditions

As to edge plasma parameters, there was unfortunately no direct measurement during the course of deposition probe experiments. However, relevant edge plasma data are available from earlier measurements [12], using a reciprocating Langmuir probe, conducted for the core plasma parameters similar to those employed in this work. The edge plasma density and temperature, selected for the probe position from this database, are about 2.5×10^{12} cm^{-3} and 30 eV, respectively. Substituting these data into the sheath expressions for a floating surface in a collisionless plasma [13], the parallel energy flux density has been calculated to be about 260 W/cm^2. Assuming the perpendicular to parallel heat flux ratio to be 0.05–0.5 [14], the heat flux deposited on the probe top surface is 13–130 W/cm^2, a rather significant uncertainty. Taking into account the retained heat effect from preceding discharges, the maximum probe surface temperatures have been calculated to be 450°C, 570°C, 667°C, and 579°C, respectively, during the four lithium-pellet injected discharges for the deposition probe measurements [15].

3.2. Deposition probe materials analysis

3.2.1. Surface appearance and microscopic morphology analysis with SEM

The deposition probe after the plasma exposure in TFTR is shown in Fig. 1. Notice that there is clearly a difference in appearance between the electron and ion drift sides. Due to the machine configurations resulting in shadowing effects in several areas, the heat deposition on the e-side is predicted to be higher than that on the i-side for a limiter-like structure inserted from the Bay-D port. Consistent with this prediction, the e-side surface appears to be burned and sooty, indicating high-temperature erosion, whereas the i-side suggests a rather mild erosion condition.

These macroscopic observations are compared with microscopic analysis with SEM. Shown in Fig. 2(a)–(f) are the electron micrographs of the probe surfaces, perpendicular and parallel to the fiber bundle weaving direction. Compared with as-machined surfaces, rather strong surface modifications are seen on all exposed surfaces. On the e-side perpendicular surface, shown in Fig. 2(c), protruding nodular structures are observed. These are eroded fiber bundles with deeply etched boundaries. Similar nodular structures have been observed in other tokamak experiments [16]. One also finds that some of the fiber bundles on the e-side parallel surface, shown in Fig. 2(d), are even torn apart due to plasma-induced erosion.

In contrast, scale-like structures are observed on the i-side surfaces, shown in Fig. 2(e) and (f), indicative of incomplete film deposition. Discontinuous features such as these scales or islands are often observed at early stages of film deposition where the film thickness is not great enough to cover the initial surface roughness of the substrate. Because the probe was exposed to only a few discharges, the incompleteness of film coverage is highly possible.

Interestingly, the surface morphologies observed on the outboard are similar to those on the e-side. Also, similarities are found between the inboard and i-side surface morphologies. These findings are suggestive of particle and heat flows, crossing over the deposition probe at the characteristic angle, related to the toroidal magnetic field guiding center shown in Fig. 1(a). Corroborating this argument, the scale-structures observed on the i-side appear to 'wave' in one particular direction.

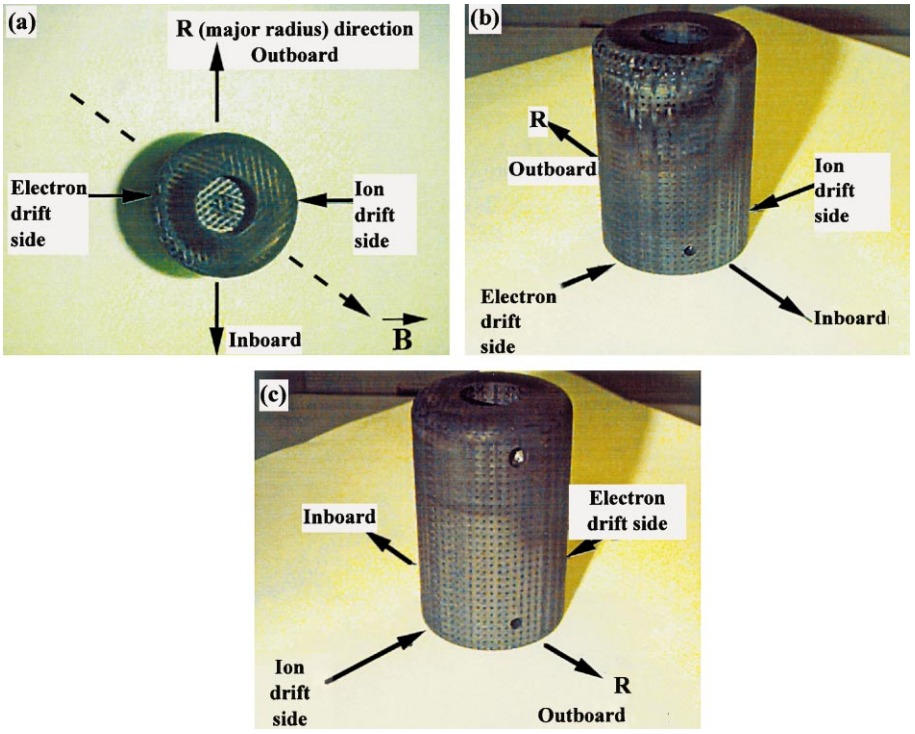

Fig. 1. The deposition probe after TFTR plasma exposure.

Further details on the particle transport is beyond the scope of this paper.

3.2.2. Deuterium and lithium mapping by NRA

As shown in Fig. 3(a) are the results of NRA radial mapping of deuterium and lithium on the plasma-front surface as a function of distance from the outer edge. The probing depth in this analysis is about 1 μm. Notice that the i-side contains significantly larger amount of deuterium and lithium than the e-side, while these concentration profiles generally increase towards the center. This is believed to be related to the temperature differences between the i-side and e-side and also between the outer edge and center because the retention of hydrogenic species in carbonaceous materials is well known to decrease as temperature increases [17]. Because of its low melting point of 180.7°C, resulting in a tendency of evaporation, the retention of lithium is expected to behave similarly to that of deuterium. In addition to the thermal effect, codeposition is considered to have contributed to the increase in deuterium and lithium retention on the i-side.

The distribution profiles along the side wall in the minor radius direction are shown in Fig. 3(b). Similarly to the plasma-front surface, considerably more deuterium and lithium are detected in the i-side than in the e-side near the top surface. Again, this is presumably due to the temperature and codeposition effects. However, the opposite trend is found as the distribution curves intersect each other towards the bottom of the probe. This finding has not yet been clearly explained although one suspects some transition taking place in the plasma-surface interaction behavior along with increasing the plasma minor radius.

3.2.3. Elemental analysis with SIMS

Specimens cut from the e-side and i-side of the plasma-front surface of the probe were analyzed with both positive and negative ion SIMS, using an 5 keV argon ion beam as the probe beam. Shown in Fig. 4(a) and (b) are the positive and negative SIMS spectra, respectively, both from the i-side specimen. Caution must be taken in interpreting these spectra because peak intensities are not necessarily proportional to elemental concentration on the surface.

In the positive SIMS data, shown in Fig. 4(a), one finds most of the predictable elements and their isotopes, including hydrogen, lithium, carbon, together with some metallic impurities such as iron and chromium. In addition, sodium and potassium are detected at rather high intensities. Alkaline metals tend to generate high intensity peaks in positive SIMS, due to their low ionization potentials [18]. Also, as shown in Table 1, the CFC material used for the probe contains relatively large

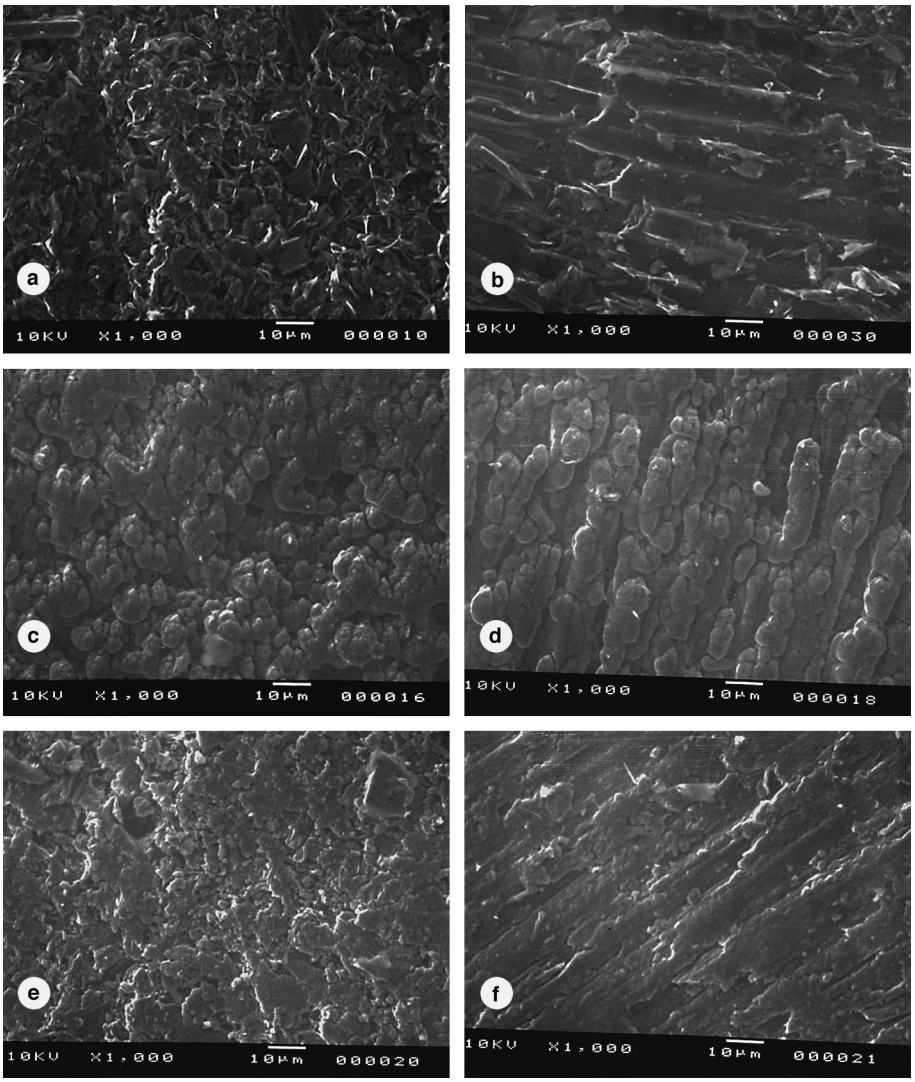

Fig. 2. Scanning electron micrographs: (a) as-machined surface perpendicular to the fiber bundles; (b) as-machined surface parallel to the fiber bundles; (c) e-side exposed perpendicular surface; (d) e-side exposed parallel surface; (e) i-side exposed perpendicular surface; and (f) i-side exposed parallel surface.

amount of ash impurities. Therefore, we do not consider that these alkaline impurities are from TFTR.

Concerning the details on SIMS data, both Li-6 and Li-7 are detected but the intensity ratio is about 10, a factor of about two off from the enrichment ratio in the injected lithium pellets. As pointed out in the previous section, this deviation is believed to be due to the contribution of recycling Li-7 from the first wall. Unlike other metal hydrides [19,20], no clear peak is found indicative of LiH^+ or LiD^+. Lithium hydride is a line compound in the phase diagram and the solid solution is mostly in the liquid phase at temperatures above the lithium melting point [21]. As a result, lithium and hydrogenic species are not strongly bound in the i-side codeposited materials. Instead of hydride, one finds several indications of oxides at $M/e = 28$ for $^6Li\ _2O^+$, 29 for $^6Li^7LiO^+$ and 30 for $^7Li\ _2O^+$, the chemistry of which will be discussed in the following section.

Interestingly, the peaks suggestive of CH^+, C_2H^+, CD^+ (or CH_2^+), and C_2D^+ (or $C_2H_2^+$) are seen in the spectra, indicating the bonding between carbon and hydrogen isotopes. This is quite consistent with the conjecture on codeposited materials of carbon and hydrogenic species. Also detected are peaks suggestive of C^6Li^+, C^7Li^+, $C_2^6Li^+$, $C_2^7Li^+$, $C_3^6Li^+$, and $C_3^7Li^+$, which may be from metastable intercalation compounds such as C_6Li or from the line compound carbide, αCLi [21].

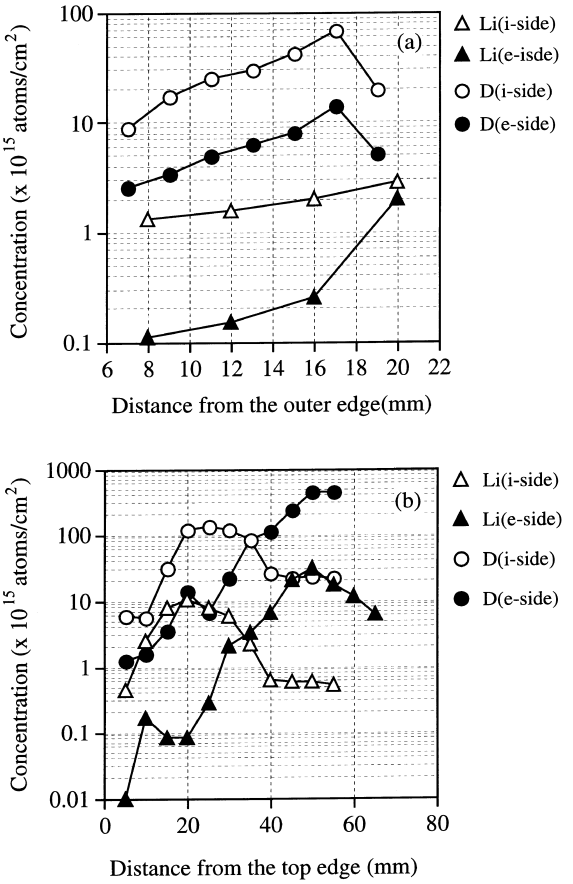

Fig. 3. Lithium (^{7}Li) and deuterium mapping by NRA on (a) plasma-front surface radial profiles; and side wall profiles along the probe major axis (b). The depth of analysis is of the order of 1 μm.

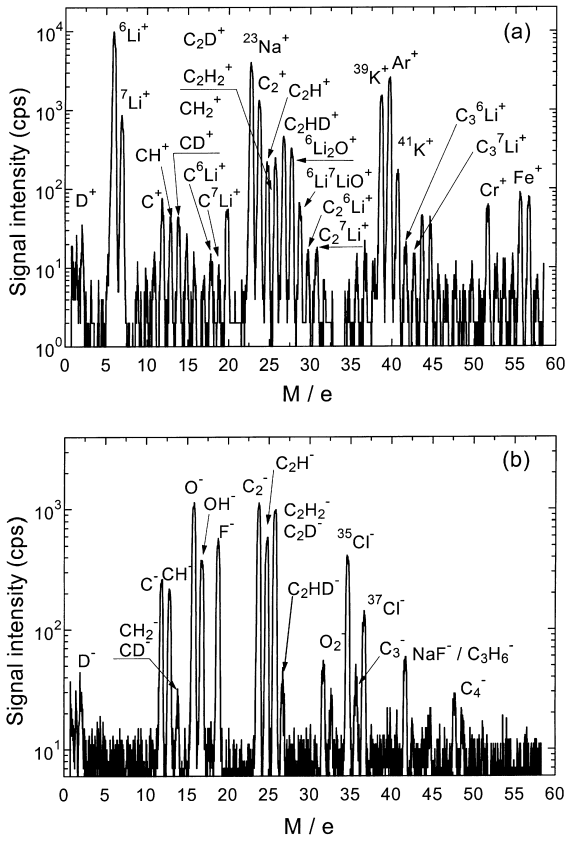

Fig. 4. SIMS analysis data on the ion-drift side codeposited materials (a) positive ion spectra; and (b) negative ion spectra.

Interestingly, these peaks are not seen in the e-side surface data (not reported). Nonetheless, the question remains open as to in what form lithium exists in the codeposited materials.

Turning to negative SIMS data, shown in Fig. 4(b), again, caution needs to be taken because several halogen elements are detected at high intensities, due to their high sensitivities to negative SIMS. In fact, chemical analysis of the raw material indicates an ash content of about 60 ppm, including these halogen elements (see Table 1). Therefore, we do not consider high-intensity halogen peaks in negative SIMS data to be pertinent with the TFTR plasma exposure. The detection of CH-, CD-compound ions supports the above-mentioned carbon hydride argument. Also, oxygen is believed to be a constituent of codeposited materials, as will be discussed in the XPS analysis, though part of it is due to air exposure.

To minimize the surface effect on SIMS data, depth profile data were taken. Shown in Fig. 5(a) are the data on lithium, $^{6}Li^{+}$ normalized by $^{12}C^{+}$, down to the depth of about 0.1 μm. In the time-to-depth conversion, the averaged atomic spacing of 6.69 Å for the *c*-axis and 2.5 Å for the *a*-axis are used because the probe material has a four-directionally woven fiber bundle structure and the argon ion beam diameter (1 mm) is large enough to sputter bundles in all directions. Again, data indicate that the i-side contains more lithium than the e-side. Also, notice similarities between the e-side and outboard, and between the i-side and inboard surfaces. This is the same trend as that was observed in surface morphologies with SEM.

The e-side specimen was subjected to deeper profiling and the result is shown in Fig. 5(b). Lithium, deuterium and oxygen are detected even at the depth exceeding 10 μm, at which depth the surface roughness effect is not quite important (see Fig. 3). As mentioned earlier, there was no direct surface temperature measurement on the probe. To evaluate these depth data, we assume that the e-side surface is maintained at the maximum temperatures for 3 s for the first three discharges and for 0.5 for the last one (see Section 3). Due to the four-directional structure, it is virtually impossible to find in literature

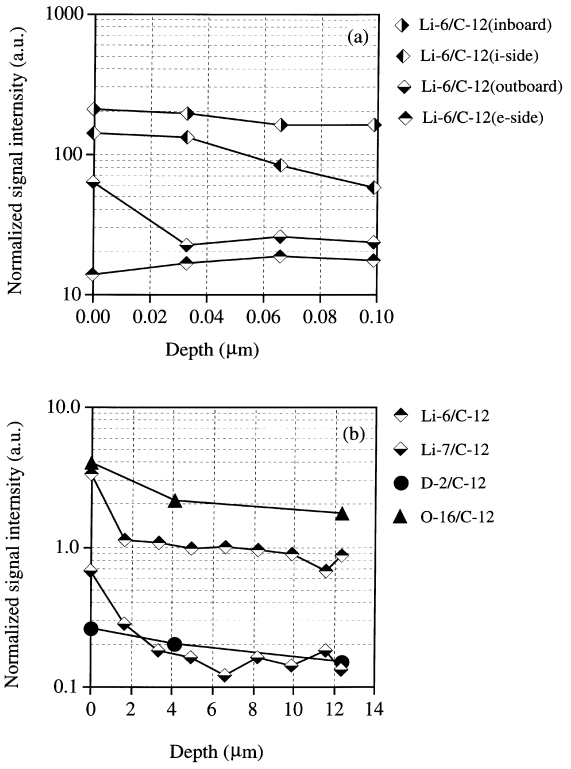

Fig. 5. SIMS depth profile analysis (a) ^{6}Li profiles for electron, ion, inboard and outboard side surfaces; and (b) deeper profiles into the electron side eroded surface. Data are normalized by the signal intensity of $^{12}C^{+}$, chosen as the internal reference. However, this normalization does not necessarily allow us to compare other materials in quantity because of the difference in secondary ion emission efficiencies of individual elements.

the exact data needed here. Nonetheless, the diffusivity of lithium in pyrolytic graphite, D_{Li} (cm^2/s) $= 3 \times 10^3$ exp (−1.83 (eV)/kT) [22], reported for the basal plane direction is relevant because carbon hexagonal planes within an individual fiber are aligned in parallel. The total characteristic diffusion length, given by the sum of $\sqrt{Dt}$ where D is diffusivity and t is time, has been calculated to be about 16 μm, which is of the same order as the SIMS depth data. As to deuterium penetration, the tritium diffusivity reported for a three-directional CFC, D_T (m^2/s) $= 1.72 \times 10^{-8}$ exp (−52.531 (kJ/mol)/RT) [23], is used and the total characteristic diffusion length has been calculated to be 18.5 μm. Using the ratio of $\sqrt{m_T/m_D}$, this diffusion length for tritium has been corrected to be 22.6 μm for deuterium, which is, again, of the same order as the SIMS depth data. As for oxygen penetration, unfortunately, diffusivity data are not available under relevant conditions. There are two possibilities, however: the attachment of oxygen to the metastable lithium-intercalated graphite structure and/or the formation of another intercalation compound such as C_8O_2OH [24]. Further discussion on this subject is beyond the scope of this work.

3.2.4. Surface chemistry analysis with XPS

In this section, the surface chemistry analysis with XPS is discussed. It is important to mention here to avoid confusion that compared with that by SIMS, the sensitivity of lithium detection by XPS is significantly smaller. In the following XPS data, therefore, lithium is not seen. Nonetheless, it is possible to investigate the chemistry of it from the valence electron binding energy analysis on other elements such as oxygen and carbon, having reasonably high sensitivities for O1s and C1s, respectively.

The results of binding energy analysis are shown in Fig. 6(a)–(d). Oxygen is detected on the as-machined surface but at a significantly lower intensity, compared with that on the i-side surface. This is believed to be due to air exposure. Therefore, we consider that most oxygen detected on the e-side and i-side is from TFTR. For more detailed binding energy analysis, O1s peaks have been deconvoluted into component peaks, those of which shown in Fig. 6(c) are taken from the i-side specimen. These component peaks are related to oxygen bound in the form of –OH, CO– and M_xO_y (metal-oxide). Correlated to the SIMS data, the most likely metal for the M_xO_y compound is lithium. From the areas below these peaks and wide energy range data [10], the concentration of lithium is estimated to be a few percent. This is significantly less than the averaged lithium coverage of 1 monolayer (see Section 2). However, considering the diffusion effects inward and perhaps outward as well, leading to materials mixing, this small concentration in the i-side codeposits is not totally surprising. Similar XPS analysis on the e-side specimen has resulted in even less lithium than this, which is consistent with the SIMS data (see Fig. 5(a)) and also the NRA data (see Fig. 4(a) and (b)).

Turning to carbon chemistry data, shown in Fig. 6(b) and (d), the major component peak is due to carbon in the graphite crystalline, both for the as-machined and i-side specimens. The other peak, much pronounced on the i-side specimen, is believed to be due to carbon compounds in the form of –CH_2–, –CO and –COH. These are believed to illustrate the carbon chemistry in the codeposited materials although air exposure which may have contributed to an extent. Not having a covalent bonding, no clear sign of C_6Li is seen in the XPS data. The corresponding peaks observed on the e-side are significantly smaller (data not reported here).

3.2.5. Spontaneous tritium release

Immediately after plasma exposure, the probe was subjected to smear tests for tritium monitoring at PPPL. The total tritium content over the probe surface was estimated to be 30 μCi. However, it was instructed in

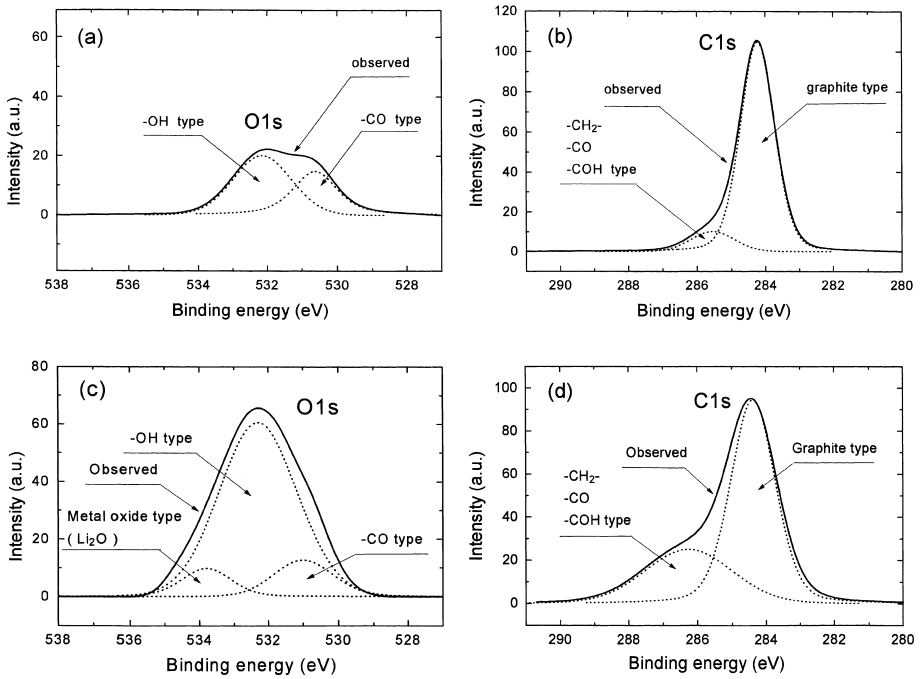

Fig. 6. XPS analysis data on oxygen (O1s) and carbon (C1s) electron binding energies: (a), (b) as-received FMI C–C composite material; and (c), (d) ion side codeposited materials on the probe. As opposed to the SIMS data, one can quantitatively analyze the composition, using the areas defined below these deconvoluted curves.

these tests that the plasma-interacted areas not be affected for the sake of subsequent materials analysis. The smear samples were thus taken from the bottom of the probe (Fig. 1). We suspect that this instruction has led to the underestimation of tritium contents.

It has often been observed that graphite materials implanted with hydrogenic species decomposes in moist air even at room temperature but the rate decays rather rapidly [25]. Two months after plasma exposure, however, the probe radioactivity was found to be much higher than expected at the time when NRA was performed at SNL, penetrating a vinyl glovebox wall with a thickness of about 2 mm within a day or so.

Three months later at Toyama University, we observed significant tritium release upon opening the argon-packed container. Tritium release was even more pronounced, exceeding 10 pCi/cm^3 in a glovebox, while the probe was sliced into small specimens for the SIMS-XPS analysis. Afterwards, further cuttings were done on these specimens in order that the amount of tritium was absolutely evaluated using the combustion method. Results are: 2.4 μCi/g in the e-side; 4.0 μCi/g in the i-side; 3.5 μCi/g in the outboard; and 11 μCi/g in the inboard [11]. From these data, one expects the total tritium content exceeding the initial on-site smear test data by orders of magnitude. Interestingly, however, tritium was not detected in thermal desorption measurements conducted for a specimen sectioned from the i-side side wall (Fig. 3) up to about 900°C [26]. This is primarily because the gas detection limit is 10^{-9} Torr and also because the noise level is relatively high due to the previous use with tritium-containing gases in the same facility.

Four months later at UCSD during the course of SEM analysis, no tritium release was observed with the detection limit of 5 pCi/cm^3. Smear tests conducted along with facility decontamination have indicated that there is essentially no tritium contamination, other than the surfaces directly in contact with the specimens, inside as well as outside the vinyl glovebox. Although as such, radioactivity measurements have not always been quantitative in this work, our observations suggest that immediately after TFTR exposure the probe may have contained tritium of the order of 1 mCi and thus the radioactivity took almost a year to decay.

4. Summary and the hypothesis of lithium-conditioned wall mechanism

This work has presented the first set of materials analysis data on an edge probe exposed to TFTR plasmas with lithium pellet injection. The probe has been found to be deposited with particle and heat fluxes in the manner that shows the flow direction characterized by

the magnetic configuration. The i-side surface exhibits a clear sign of codeposition of carbon, lithium, deuterium, oxygen, etc. whereas the e-side indicates high-temperature erosion. Despite its high reactivity to form various compounds, lithium has been detected only in the form of oxide in these codeposits. This solid-phase chemistry can perfectly be explained by the Gibb's free energy of formation argument in classical thermodynamics. However, we conjecture more non-equilibrium nature in the interaction of lithium-coated walls with edge plasma environment. The indications of metastable graphite intercalation compounds may be a reflection of this aspect.

In recent experiments related to materials mixing, carbon deposits have been observed to be mixed up with substrate beryllium, via outward diffusion, at elevated temperatures [27,28]. One extrapolates from this that if the host material is lower-Z than deposits, diffusion can be outward as well as inward to mix materials. Carbon walls with lithium coatings provide an interesting opportunity for such materials mixing. Even if it is covered with arriving impurities, lithium may be able to penetrate deposits to create a new surface, as long as the wall temperature is high enough to drive diffusion mixing. When it is sputtered, lithium is likely to be self-redeposited, not being able to overcome the sheath potential, due to its high efficiency of secondary ion formation [29]. This not only reduces erosion loss but maintains surface gettering.

Consistent with this hypothesis, the enhanced supershot mode operation in TFTR requires lithium coatings on the bumper limiter, particularly in the area off the mid-plane, where the surface temperature is relatively high due to heat deposition [30]. This temperature effect partially explains recent observations that tokamaks running divertor discharges do not seem to benefit significantly from lithium wall conditioning because plasma-interactive surface temperatures are claimed to be controlled as low as room temperature. These arguments suggest that the key mechanism to successful lithium wall conditioning may be materials mixing in codeposits at optimized wall temperatures. Unfortunately, however, we can not be any more conclusive than this due to the shutdown of TFTR.

Acknowledgements

This work is funded by the Princeton University, the US Department of Energy, and also the Ministry of Education of Japan. Special thanks goes to the safety staff members, including B. Elkin at SNL and S. O'brien at UCSD.

References

[1] H.F. Dylla et al., J. Nucl. Mater. 162–164 (1989) 128.
[2] G.L. Jackson et al., J. Vacuum Sci. Technol. A 10 (1992) 1244.
[3] J.L. Terry et al., Proceedings of the 13th International Conference on Plasma Physics and Controlled Nuclear Fusion Research, Washington, USA, 1990, p. A–V–5.
[4] D.Mansfield et al., Phys. Plasmas 3 (1996) 1.
[5] J. Winter et al., J. Nucl. Mater. 162–164 (1989) 713.
[6] G.L. Jackson et al., J. Nucl. Mater. 241–243 (1997) 655.
[7] H. Sugai et al., J. Nucl. Mater. 220–222 (1995) 254.
[8] B. Terrault et al., J. Nucl. Mater. 220–222 (1995) 1130.
[9] J.L. Terry, Lithium wall conditioning of metal walls in alcator C–Mod, presented at the Workshop on Lithium Effects in Plasmas, 17–18 October 1996, Princeton, Workshop summary published in Nucl. Fusion 37 (1997) 705.
[10] K. Ashida et al., Surface characterization of TFTR graphite probe by XPS-SIMS, Annual Report of Hydrogen Isotope Research Centre, Toyama University, vol. 17, 1997, in press.
[11] M. Hara et al., Analysis of tritium implanted in an edge probe in TFTR, ibid.
[12] C.S. Pitcher et al., Nucl. Fusion 32 (1992) 239.
[13] P.C. Stangeby, in: D.E. Carslaw, J.C. Jaeger (Eds.), Physics of Plasma-Wall Interactions in Controlled Fusion, Plenum Press, NATO ASI Series vol. 131, 1984.
[14] P.C. Stangeby et al., Nucl. Fusion 32 (1992) 2079.
[15] H.S. Carslaw, J.C. Jaeger, Conduction of Heat in Solids, Clarendon, Oxford, 1959.
[16] Y. Hirooka, R.W. Conn, in: R.K. Janev, H.W. Drawin (Eds.), Atomic and Plasma-Material Interaction Processes in Controlled Thermonuclear Fusion, Elsevier Science, Amsterdam, 1993.
[17] R.A. Causey, J. Nucl. Mater. 162–164 (1989) 151.
[18] C.A. Andersen, J.R. Hinthorne, Ana. Chem. 45 (1973) 1421.
[19] K. Ashida et al., J. Nucl. Mater. 210 (1994) 233.
[20] Y. Hirooka et al., J. Nucl. Mater. 114 (1983) 341.
[21] T.B. Massaski (Ed.), Binary Alloy Phase Diagrams, 2nd ed., vol. 2, ASM International, Metals Park, OH, 1990.
[22] B. Jungblut, E. Hinkis, Phys. Rev. B 40 (1989) 10810.
[23] S. alberici et al., Fusion Technol. 28 (1995) 1108.
[24] F.A. Cotton, G. Wilkinson, Advanced Inorganic Chemistry, 5th ed., Willey, New York, 1988.
[25] S. Chiu, A.A. Haasz, J. Vac. Sci. Technol. A 9 (1991) 747.
[26] K. Ashida et al., Surface Analysis of TFTR Graphite Probe and Thermal Desorption of Gases, presented at the Japanese Atomic Energy Society Meeting, Osaka, 2–28 March 1998.
[27] Y. Hirooka et al., J. Nucl. Mater. 230 (196) 173.
[28] K. Ashida et al., Fusion Eng. and Design, special issue Beryllium studies for fusion, part-1, 37 (1997) 307.
[29] A. Krauss et al., J. Nucl. Mater. 103 & 104 (1981) 239.
[30] D.K. Mansfield et al., Lithium Conditioning Experiments on TFTR: An Overview, presented at the same workshop as Ref. [9].